



Exploring Radiation's Effects on Lung Cancer, with a focus on Motility and Migration

Citation

Moorhead, Graydon. 2022. Exploring Radiation's Effects on Lung Cancer, with a focus on Motility and Migration. Bachelor's thesis, Harvard College.

Link

<https://nrs.harvard.edu/URN-3:HUL.INSTREPOS:37372704>

Terms of use

This article was downloaded from Harvard University's DASH repository, and is made available under the terms and conditions applicable to Other Posted Material (LAA), as set forth at

<https://harvardwiki.atlassian.net/wiki/external/NGY5NDE4ZjgzNTc5NDQzMGIzZWZhMGFIOWI2M2EwYTg>

Accessibility

<https://accessibility.huit.harvard.edu/digital-accessibility-policy>

Share Your Story

The Harvard community has made this article openly available. Please share how this access benefits you. [Submit a story](#)

Exploring Radiation's Effects on Lung Cancer, with a
focus on Motility and Migration

A thesis submitted by

Graydon Moorhead

To

Applied Mathematics

in partial fulfillment of the honors requirements

for the degree of Bachelor of Arts

Harvard College

Cambridge, Massachusetts

March 25, 2022

Abstract

Lung cancer is one of the deadliest forms of cancer. A common therapeutic agent is radiation, but there is beginning to be more and more evidence about how radiation can actually have effects on motility and migration, increasing the risk for metastasis. To explore this, a model of lung cancer was built using A549 cells. It was found that high dose, intensive hypofractionated radiation schedules can lead to more cell death, but have the effect of leaving the tumor in a highly dispersed state as compared to lower intensity, hyperfractionated radiations schedules.

Acknowledgements

This project has been quite a journey for me, but I simply could not have done it without the advice and support of Postdoc Danny Temko, who was with me every step of the way from start to finish. Looking back at my time with him, we consistently met twice a week for almost a year, and I can't thank him enough for the time and effort he put into helping me delve into this project.

Secondly, I must thank Professor Franziska Michor. Her compassion and expert advice helped direct this project into what was the unknown for me. I am extremely grateful for the time I have spent in her lab, as it has allowed me to progress as a researcher in ways I never thought possible.

My support system of friends is simply amazing and I appreciate every one of you who has either given feedback, advice, support, or simply allowed me to talk about my project. Words can't express my thanks. To name but a few in no particular order, I must thank Mia, Evans, Manu, Ilai, Alicia, Logan, Brandon, Ben, Paul, Isabel, Nik, and Fari. A special shoutout to Richard and Chloe for helping me with Latex, BibTex, and some statistics.

Finally, I must thank my parents, who have supported me throughout my life and pushed me to be the best that I can be. I love you both.

Contents

1	Introduction	11
1.1	A549 Cells	11
1.2	Radiation and Cellular Movement	13
1.3	The Model	15
1.4	Radiation Optimization Example	16
2	Proposed Model	19
2.1	General Overview	19
2.2	Initial Conditions	20
2.3	Inter-cellular Interactions	20
2.4	Cell Cycle	20
2.5	Cell Death	21
2.6	Cellular Movement	22
2.7	Model Analysis	24
3	Results	25
3.1	Replicate Analysis	25
3.2	Exploration of Practical Radiation Schedules	26
3.3	Comparison of Hypo and Hyperfractionated Radiation Schedules	30
3.4	Sensitivity Analyses	33
3.5	Optimization Algorithm	35
3.6	Negative Slope Analysis	38
4	Conclusion	41
4.1	Further Directions	42

List of Figures

1.1	Structure of the Alveolus [1]	12
1.2	Progression of Alveolar Type II Epithelial Adenocarcinoma [2]	13
1.3	Pathway of Metastasis [3]	15
2.1	Velocity Timeline in Relation to Doses	24
3.1	Replicate Analysis of the Standard of Care Schedule	26
3.2	Caption	28
3.3	Comparison of Different Radiation Schedules. The standard of care schedule is a blue star, the various chosen schedules are in green, and the rest of the random schedules are in red	29
3.4	Analysis of hyper and hypofractionation. To get the upper and lower bounds of each schedule in the graph, the trials were aligned from lowest to highest dispersion at each time point. Then the upper bound was chosen as the 80th highest point and the lower bound was chosen as the 20th highest point	31
3.5	Analysis of hypo and hyperfractionated schedules in terms of both average pairwise distance and survival fraction.	32
3.6	3Gy once a day in blue, 1.5Gy twice a day in green, and 1Gy three times a day in red. Schedules run for 75 hours. Upper and lower bounds for schedules determined in the same manor as Figure 3.4	34
3.7	Progression of Simulated Annealing Algorithm	38
3.8	Average pairwise distance of tumor in response to hypo and hyperfractionated radiation schedules with a negative relationship between slope and increasing radiation dose.	39

Chapter 1

Introduction

Lung cancer is the leading cause of cancer-related deaths in men and women in the US [4]. Accounting for around 25% of all cancer-related deaths [5], the chances that a man will develop lung cancer is 1 in 15 while the chances that a woman will develop it is 1 in 17 [5]. Lung cancer has four common types: lung nodules, non-small cell lung cancer (NSCLC), small cell lung cancer (SCLC), and mesothelioma; the most common of which is non-small cell lung cancer [6]. It is important that research and modeling is done on lung cancer in an attempt to better understand and counteract this disease.

1.1 A549 Cells

One well-studied lung cancer cell line is the A549 cell line. It was cultured by D.J. Guiard et al. in 1972 from a 58-year-old male [7]. It is a type of non-small cell lung cancer, which accounts for 80% of all lung cancer [8], and develops in the form of adenocarcinoma, which develops in epithelial cells. Lung adenocarcinoma is the most common form of lung cancer

(30%) and accounts for about 40% of NSCLC occurrences [8]. In Figure 1.1, there is a diagram of an alveolar sac with different types of cells labeled.

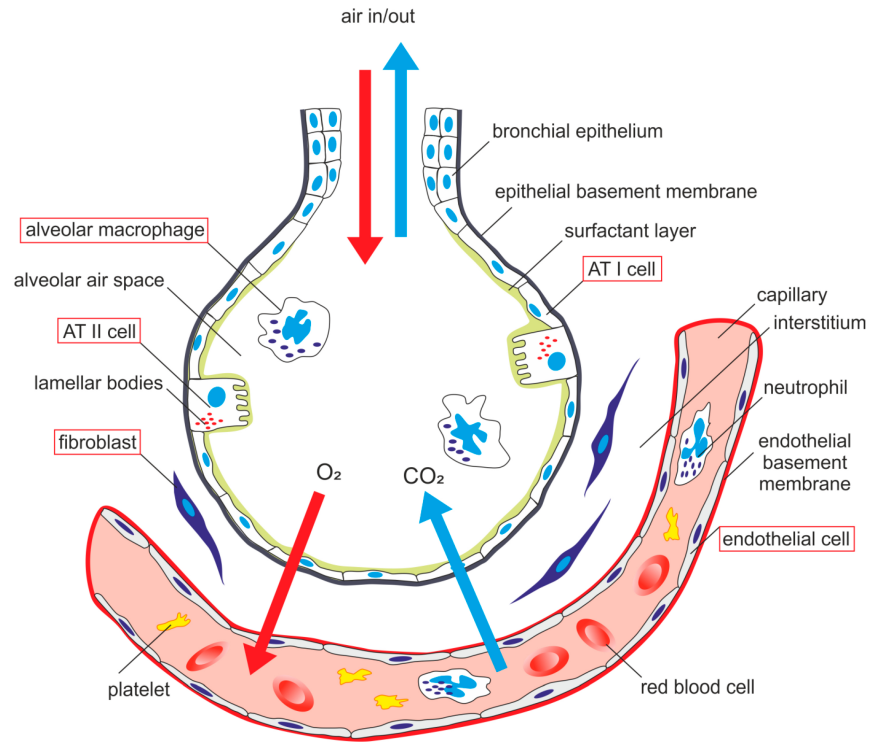


Figure 1.1: Structure of the Alveolus [1]

A549 cells are derived from alveolar type II pulmonary epithelial cells, and as seen in Figure 1.1, they make up part of the lining of the alveolar sac. Figure 1.2 is a representation of how an adenocarcinoma might develop from an alveolar type II epithelial cell. The cancer cell divides outwards and expands, surrounding one wall of the alveolus.

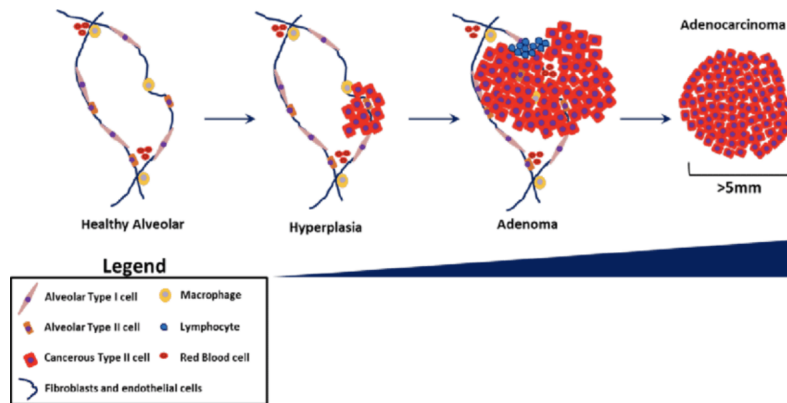


Figure 1.2: Progression of Alveolar Type II Epithelial Adenocarcinoma [2]

1.2 Radiation and Cellular Movement

Radiation is one of the most common forms of therapy: around 50% of cancer patients receive it as a form of treatment [9] and it is estimated that it contributes around 40% of curative treatment [10]. However, there are aspects of radiation that can have major consequences. There are proposals, for example, that radiation can induce metastasis, although there isn't definitive evidence that this is true [11]. The A549 cell line is one specific cell in which radiation causes significant effects outside of cell death.

In a study by Ishihara et al., they demonstrated that irradiation-tolerant A549P-3 cells indicate high invasive activity in vitro. They demonstrated this by taking A549 cells that have survived radiation and doing a 2D motility and 3D migration assay, comparing them to normal A549 cells. In addition, irradiation-tolerant A549 cells (A549-3IR) displayed a spindle morphology while A549P-3 cells displayed round morphology in collagen gel overlay assay (Ishihara et al.). This change in morphology in the A549 irradiation-resistant cells probably indicates an epithelial-mesenchymal transition (EMT) [12].

In a study by Jung et al., they found that radiation-induced increased migration of A549 cells associated with EMT seems to be linked to radiation-induced fibrosis. They demonstrate that “stress fibres and focal adhesions are increased and that cell-cell junctions are decreased in response to ionising radiation” [13]. In a similar fashion to Ishihara et al., they found that radiation “significantly increased cell motility”. In the study, they also identify that SB203580 (a p38-specific inhibitor) reduces radiation-promoted migration along with SP600125 (JNK MAPK-specific inhibitor), which also inhibited inherent cell motility. Additionally, they demonstrate that radiation up-regulates p38 MAPK. Jung et al. ultimately suggest that some patients may benefit from inhibitors of EMT or cellular migration combined with radiotherapy [13].

The issue with an increase in cellular motility is that motility is important for metastasis [3], or the spreading of cancer cells to other areas of the body. One possible explanation for this is EMT. When cells acquire mesenchymal characteristics, they have increased migratory capabilities and decreased cell-cell adhesion (a characteristic of A549 following radiation found in Jung et al.). Upon landing at a new site, cells then undergo MET, or mesenchymal-epithelial transition, to reattach and resume proliferation [14] [15] [16] [17]. Figure 1.3 illustrates how metastasis works.

Additional research has been done into quantifying the effects that radiation has on various cell lines. In an unpublished study that was a joint effort between the Michor and Lahav labs, a number of cancer cell lines, among them the A549 cell line, were analyzed in their motility response to radiation. The cell lines were exposed to different amounts of radiation and then monitored for 24 hours with pictures being taken of the cells every 15 minutes. From this data, they were able to plot the distribution of cellular velocity in response to different amounts of radiation [18].

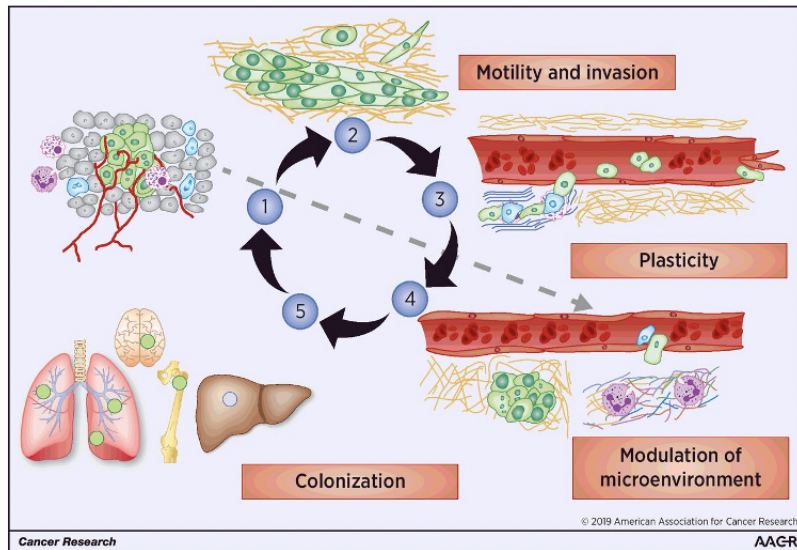


Figure 1.3: Pathway of Metastasis [3]

1.3 The Model

To further explore this area of radiation and its effects on motility, I built a model of lung cancer largely based off of A549 cells. Although the A549 cell line is not necessarily a model cell line for all lung cancer, as all cell lines are unique, it has benefits of being well-studied, especially in relationship to its response to radiation. It is therefore a great starting place from which to explore how radiation effects lung cancer motility.

The idea behind the model is to explore radiation schedules and their effects on motility, looking specifically at survival fraction and cellular movement in the tumor following a specific radiation schedule. In order to quantify cellular movement, the dispersion of the tumor is used as a summary statistic of how much cells have moved throughout the time course of the simulation. In this project, average pairwise distance of cells is used as a method to calculate spatial dispersion. Therefore, the goal of this project is to build a model of lung cancer and analyze different radiation schedules with respect to survival fraction and

average pairwise distance of the tumor cells, and furthermore performing optimization to find a schedule that effectively kills the tumor while minimizing tumor dispersion.

1.4 Radiation Optimization Example

The proposed model in this project is influenced by a similar model built by Randles et al. on glioblastoma. To provide context for the proposed model, a summary of the Randles et al. model is provided below.

Amanda Randles et al. introduce a spatial-temporal tumor model that can effectively model chemo-radiation therapy for glioblastoma. The micro-environment that is modeled is the perivascular niche. Due to its geometry, it was modeled as a 2D cross-section with the blood vessel in the middle and the tumor stem cells surrounding the vessel. The model is set up such that the stem cells remain in place, and divide and differentiate outwards, away from the central blood vessel. There are two types of cancer cells in the model: stem-like resistant cells and differentiated sensitive cells. The general workflow of the model is that a dose of radiation is applied and cells die/survive following a linear-quadratic model. Stem-like resistant cells are more likely to survive. Following radiation, all of the surviving cells undergo quiescence for DNA repair. This quiescent period lasts for 24 hours plus an exponentially distributed random variable. When a dose of chemotherapy is applied, the drug diffuses out of the blood vessel to the surrounding tumor and kills cells with a certain probability that is also dependent on the type of cell (either stem-like resistant or differentiated sensitive) [19].

In order to then find optimal radiotherapy dosing schedules, they set some restraints on radiation schedules, with help from “information of the Brigham and Women’s Hospital/Dana-Farber Cancer Institute radiation oncology clinic for potential clinical translation in the fu-

ture” [19]. The restraints were that radiation could only be administered Monday to Friday between 08:00 and 17:00, but there could be no more than 8h between the first and last dose in a day. There could be a maximum of three doses in a day, and each dose had to be administered on the hour. In terms of the doses themselves, the maximum dose at a time was 3Gy and the maximum total dose allowed to be given in a day was 4Gy [19].

Randles et al., then set a constant chemotherapy schedule and then ran a simulated annealing optimization algorithm to find the optimal radiation schedule that fits the chemotherapy schedule. Each possible schedule was run 128 times. They then took the optimal radiation schedule that they calculated and verified its efficacy in a mouse model versus the standard of care for glioblastoma. They found that their optimized schedule increased the survival rate of the mice [19].

Chapter 2

Proposed Model

2.1 General Overview

The proposed model was built in c++ using a program called Chaste. The model was built using the cell-based package and is an agent-based model, meaning that each cell is its own object and is treated as an individual entity, rather than a holistic simulation of an entire tissue/tumor. The model has a discrete time-stepping workflow, in which there is a set time step between loops. At each computational loop, the simulation computes what happens in the next time step, such as cell cycle changes, division, death, and movement. In similar fashion to the Randles et al. model, the model exists in 2D space [19]. However, unlike the Randles et al. model, there aren't any boundary conditions on the model [19], and the tumor can theoretically expand into infinity. The reasoning for this is so that the model can remain general, and not specific to any particular biological phenomenon.

2.2 Initial Conditions

At the start of the simulation, all of the cells are placed equidistantly in a circular mesh at a population size of 344 cells. This small initial population size was chosen to minimize memory expense, and a sensitivity analysis around this number is performed. All of the cells are uniformly assigned a birth time that is before the time of the simulation start so that when the simulation starts, there is some diversity of cell cycle amongst the cells and they will not begin to divide at around the same time.

2.3 Inter-cellular Interactions

There is a linear spring force between cells, such that when cells are extremely close to each other, they repel each other, but when they are farther apart they attract each other. Importantly, there is a cutoff distance beyond which cells cannot have attractive forces with each other. This distance is set to $1\frac{1}{2}$ multiplied by the diameter of a cell. This cutoff length is set so that cells on opposite sides of the tumor don't attract each other.

2.4 Cell Cycle

The cell cycle of each cell is split into each cell cycle phase: G1, S, G2, M. Each cell is given a normally distributed time for each phase, based on data from Hill and Skarsgaard [20]. There are two things that can change the cell cycle in the simulation: volume inhibition and radiation.

If a cell's volume becomes less than or equal to 50% of its equilibrium volume, then the cell's current phase is extended indefinitely until this volume constraint is no longer

satisfied. This is to prevent the formation of an unrealistically dense core, which can occur when cells are allowed to divide under intense volume constraints.

If a cell doesn't die following a dose of radiation, it has still received substantial DNA damage. Under these circumstances, it is common for a cell to undergo quiescence to repair itself before moving on in the cell cycle. This is modeled in the simulation by adding 24 hours plus an exponentially distributed random variable to the phase of a cell that hasn't died due to radiation. The value of 24 hours and the rate parameter for the exponentially distributed random variable are both taken from a model of glioblastoma by Randles et al. [19].

When a cell undergoes division, all of its cell cycle phase times are reset and the daughter cell is given a new set of normally distributed phase times.

2.5 Cell Death

There are two modes of cellular death in the model. The most significant one is cell death due to radiation. The survival fraction of cells are taken directly from a parameterized linear-quadratic model for A549 cells created by Hill and Skarsgaard [20]. The survival fraction is then used as a probability of death on a per-cell basis. Additionally, the created LQ model is specific to the cell cycle phase, in that there are slightly different parameters for the LQ model for the G1 phase than the G2 phase.

The other method of cell death is a constant death rate, which is small in magnitude compared to the death caused by radiation. The death rate is taken from a parameterized model of PC9 cells by Kamrine Poels et al. [21], which is a different NSCLC cell line.

2.6 Cellular Movement

In the movement response data set, it was illustrated that there was unbiased random motion of cells, of which the speed increased linearly with radiation dose. Therefore, cellular motion in the simulation is completely random and is modeled by Brownian motion. Following a dose of radiation, the speed of the cells is increased for 24 hours following the dose of radiation. The velocity of a cell is translated exactly to the simulation, in that the cellular velocity seen in the dish is the exact same velocity seen in the simulation.

In the cellular velocity data set that is being used, there is only data for 24 hours following the dose of radiation. Therefore, it is not known what happens after that time period. It was decided to end the period of increased velocity at 24 hours to align with the period of quiescence. It is a reasonable assumption that once a cell has repaired its DNA and resumed its cell cycle, its cellular movement will also return to normal.

When additional doses are given within the 24 hour period following an initial dose, subsequent doses add velocity to the cell but in a diminishing returns system. The reasoning behind the diminishing returns system is that once a cell has received radiation and has survived, in the model it undergoes quiescence, which is to model DNA and general cellular damage. When an A549 cell is in that state, according to the data [18], the cell moves faster, which could be due to a variety of reasons including DNA damage, cellular damage, or cell environmental sensing. The question is: what happens when another dose of radiation is applied before the cell has repaired itself? The prediction used in the model is that this second dose in close temporal proximity doesn't have the same effect on velocity that it would normally have on an untouched cell since the cell is already damaged and sensitized to this radiation.

In the model, the diminishing returns factor is $\frac{1}{2}$, such that two consecutive 1Gy doses lead to an ultimate velocity equal to one dose of 1.5Gy. The choice of $\frac{1}{2}$ is arbitrary, and a sensitivity analysis is performed to analyze the effects of this choice on the simulations.

The overall diminishing returns system used is explained in the following arithmetic. Let $f(x)$ be the function that outputs velocity with an input of a dose in Gy:

$$f(x) = \frac{2}{7}x + \frac{40}{7} \quad (2.1)$$

Let $D_e(t)$ return the effective dose (the dose that will be input into $f(x)$ after taking diminishing returns into account) at a time t given a D , where D is a vector of doses in Gy ordered by most recent to least recent.

$$D_e(t) = \sum_{i=1}^N factor^{i-1} D_i \quad (2.2)$$

,

where N is the total number of doses within 24 hours. Essentially, the equation for $D(t)$ is a loop over all of the doses in the previous 24 hours before a time point, and each subsequent dose is compounded by $\frac{1}{2}$ after the first dose. The effective dose is then plugged into the original equation for velocity:

$$f(x, t) = \frac{2}{7}D_e(t) + \frac{40}{7} \quad (2.3)$$

This will return the average cell velocity given a dose history. Figure 2.1 gives a visual representation of the diminishing returns system in practice.

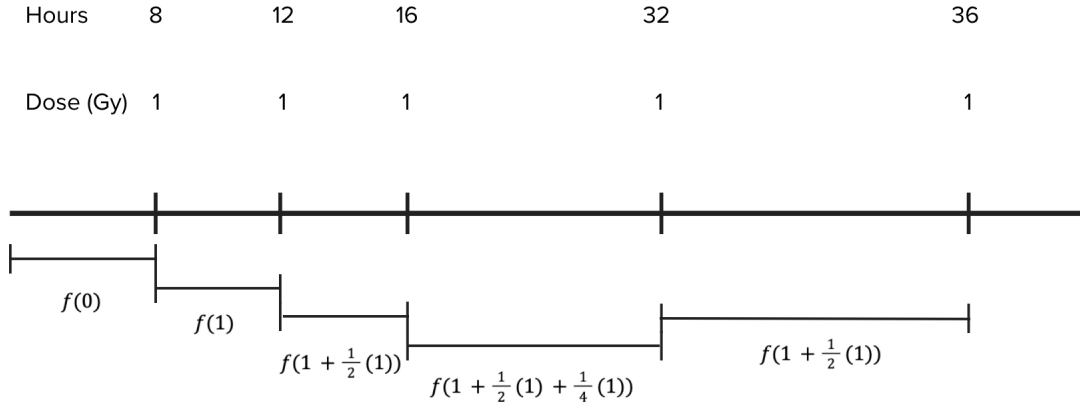


Figure 2.1: Velocity Timeline in Relation to Doses

Up to hour 8, there aren't any doses of radiation, so the velocity is $f(0)$. At hour 8, there is one dose of radiation, so the velocity is $f(1)$. Then, at hour 12, a second dose of radiation is given in close temporal proximity, so its effects on velocity are compounded by $\frac{1}{2}$, and the velocity is given by $f(1 + \frac{1}{2})$. This happens again at hour 16 to increase the velocity to $f(1 + \frac{1}{2} + \frac{1}{4})$. At hour 32, the effects of the dose at hour 8 wear off, so the velocity decreases down to $f(1 + \frac{1}{2})$.

In the model, the velocity is then converted into parameters that Chaste uses to calculate what it calls diffusion force. However, since the cells in this model aren't given a directional bias, this effectively models random Brownian motion. At each time step of the model, the random motion force is combined with cellular interaction forces to calculate the overall motion of the cell.

2.7 Model Analysis

Every 15 min, the location of every cell in the simulation is outputted to a file, which is then parsed in a python script to perform downstream analyses.

Chapter 3

Results

3.1 Replicate Analysis

To first look at the variability of the simulations, the standard of care schedule, which is 2Gy everyday [22], was run 140 times. From there, 5000 different groups were randomly chosen from the 140 standard of care replicates with replacement, and the average pairwise distance of the different groups was plotted in a histogram. The size of the groups ranged from 10 to 70, and the results can be seen in Figure 3.1. By looking at the width of the distributions comparatively, it can be seen that 30 replicates is relatively variable, but 60 replicates provides significantly more stability. For the rest of the analyses, replicate numbers in the are chosen in the range of 70 to 100.

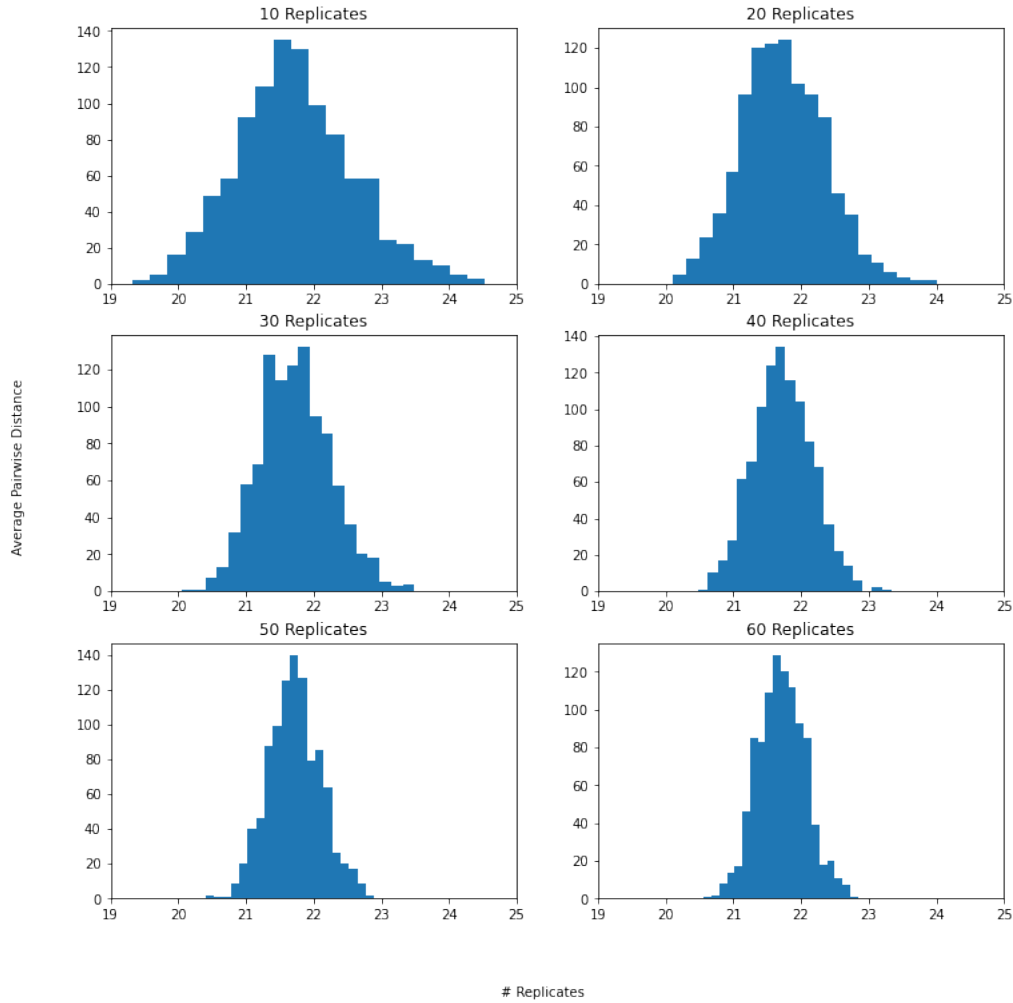


Figure 3.1: Replicate Analysis of the Standard of Care Schedule

3.2 Exploration of Practical Radiation Schedules

To explore the model I ran different 5-day schedules and compared them to each other. The constraints were based on constraints used in Randles et al. [19]. In a similar fashion, the schedules were run for 5 days starting on Monday, and radiation is only allowed to be given on weekdays. To decrease the possible parameter space, the constraint of having no more

than 3 treatments per day and having no more than 8 h between the first and last dose per day were combined to having 3 possible times for radiation treatment: 08:00, 12:00, and 16:00. The simulations started on Monday at 00:00 and then ran until 136 hours after that time. 136 hours after that time equates to Saturday at 16:00. The reason for having the simulations end on Saturday is that the effects of radiation in the model last for 24 hours, so therefore the end time of the model has to be 24 hours after the last possible dose. To align with the increasing occurrence of hypofractionation in the treatment of lung cancer [23], the single max dose per day was increased to 4Gy. To narrow the search space further, the schedules are also limited to whole numbers of radiation doses. 6 schedules were specifically chosen to be compared with each other, and then 12 other random schedules were added to the mix. The trial schedules are in Figure 3.2.

Schedule	Days	Day 1				Day 2				Day 3				Day 4				Day 5			
		8 (hr)	12	16	20	32	36	40	44	56	60	64	68	72	80	84	88	92	104	108	112
1		2(Gy)				2				2				2				2			
2		4							4									2			
3				2		2					2						2				
4		1		1		1		1		1		1		1		1		1		1	
5				3		3					2		2								
6				3		3				2						3		1			
7							1			1		2		3		1		1		1	
8				2				1		1			2			1		2		1	
9		2		1				1					1	1				2	2		
10		1	1				1	3		1		1						1		1	
11			1	2						2				1	2					2	
12		1				1	1	1			2					1		1		2	
13		1					1	3					1	2						1	
14						1	1	1		1	1	2	3	1							
15			1			1	1	2				3	1							1	
16			4								1			3						2	
17						1	3			1	2	1								1	
18			1	1		2				3				1	1	1					

Figure 3.2: Caption

Schedules 1-6 were all chosen schedules, while schedules 7-18 were all random. Schedule 1 is the standard of care for non-small cell lung cancer: 2Gy per day (SOURCE). Schedule 2 is meant to encompass the effects of a hypofractionated schedule, but since it is a 5 day schedule, it wasn't possible to have 4Gy every 2 days. Therefore, a simple 2Gy is put in on day 5. Schedule 3 is a variation of the standard of care, with the time between 2Gy doses moved around. Schedule 4 is a hyperfractionated schedule, with 2, interspersed 1Gy doses at morning and at night. Schedule 5 is meant to explore the effects of large doses in close proximity to each other. Schedule 6 explores large 3Gy doses in proximity to smaller 1Gy doses. As noted earlier, the rest of the schedules are random. The schedules were then run 70 times on different seeds compared based on percent death and sparsity of the tumor. The results can be seen in Figure 3.3

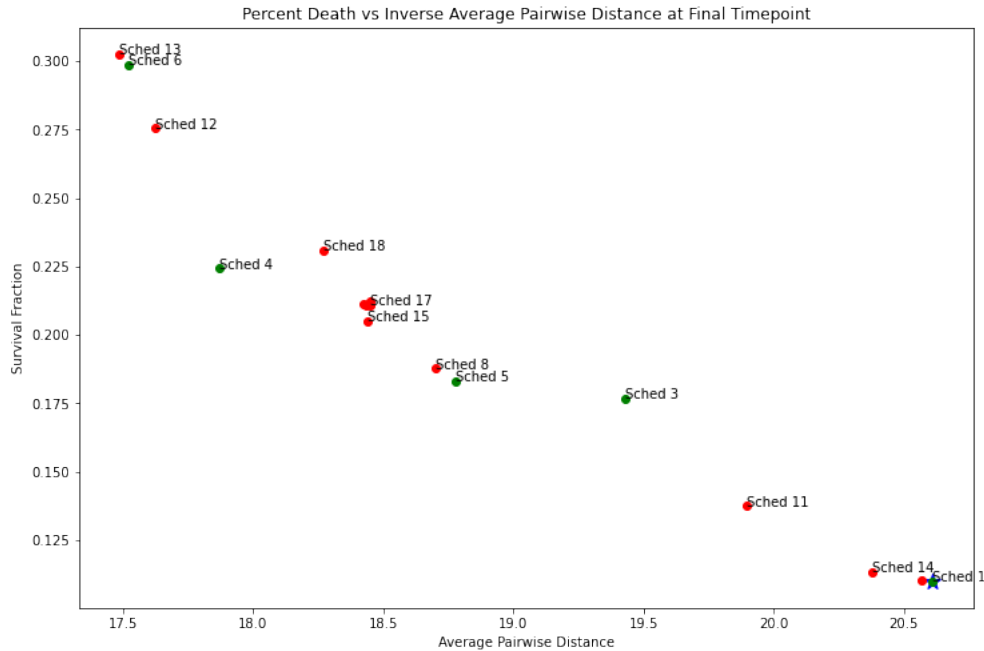


Figure 3.3: Comparison of Different Radiation Schedules. The standard of care schedule is a blue star, the various chosen schedules are in green, and the rest of the random schedules are in red

As seen in Figure 3.3, compared to the rest of the schedules, the standard of care schedule performs well in terms of percent death of the tumor. This is certainly an instance of validation for the model. In Figure 3.3, it can also be seen that there are a variety of schedules that actually perform better than the standard of care in terms of decreasing tumor dispersion, however those schedules don't perform as well in terms of killing the tumor. Although this is a small sample of the radiation schedule space, the fact that all of these schedules seem to lie along a diagonal line that starts at high survival fraction, low dispersion to low survival fraction, high dispersion, implies that there could be some sort of trade-off between the two dimensions.

3.3 Comparison of Hypo and Hyperfractionated Radiation Schedules

To investigate mechanisms of this potential trade-off, 3 schedules with the same total amount of Gy per day were devised and investigated. One schedule was 1Gy three times a day at evenly spaced intervals of 08:00, 12:00, and 16:00 (following similar restraints introduced previously), another schedule was 1.5Gy twice a day at 08:00 and 16:00, and the last schedule was 3Gy once a day at 08:00. These schedules, which break 3Gy into one large dose and also three small doses, are examples of hypo and hyperfractionation. Hypofractionation is defined as when a radiation schedule is divided into large doses. In this case, this applies to the 3Gy once-a-day schedule. Hyperfractionation, on the other hand, is defined as when a radiation schedule is split into smaller doses, and is exemplified by the 1Gy three times per day schedule. These schedules were run 100 times for 3 days. The results can be seen in Figure 3.4.

3.3. COMPARISON OF HYPO AND HYPERFRACTIONATED RADIATION SCHEDULES 31

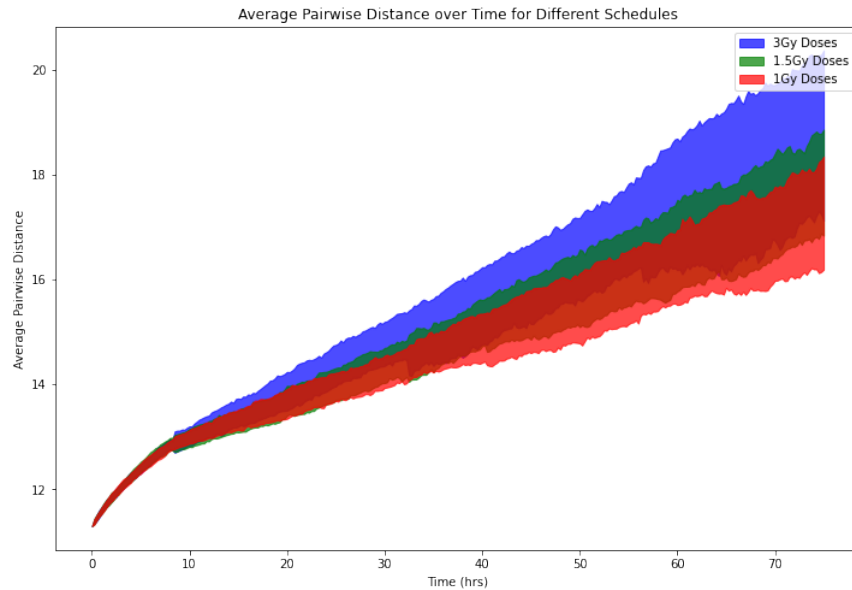


Figure 3.4: Analysis of hyper and hypofractionation. To get the upper and lower bounds of each schedule in the graph, the trials were aligned from lowest to highest dispersion at each time point. Then the upper bound was chosen as the 80th highest point and the lower bound was chosen as the 20th highest point

Based on Figure 3.4, it appears that the hypofractionated 3Gy dose schedule ends up a more dispersed tumor while the hyperfractionated 1Gy dose schedule ends with the least dispersed tumor.

In order to look at the full picture of these hyper and hypofractionated schedules, an inclusion of survival fraction of each of the trials was then included to analyze whether or not there is a trade-off between tumor dispersion and survival fraction of tumor for these schedules. The results of this are in Figure 3.5.

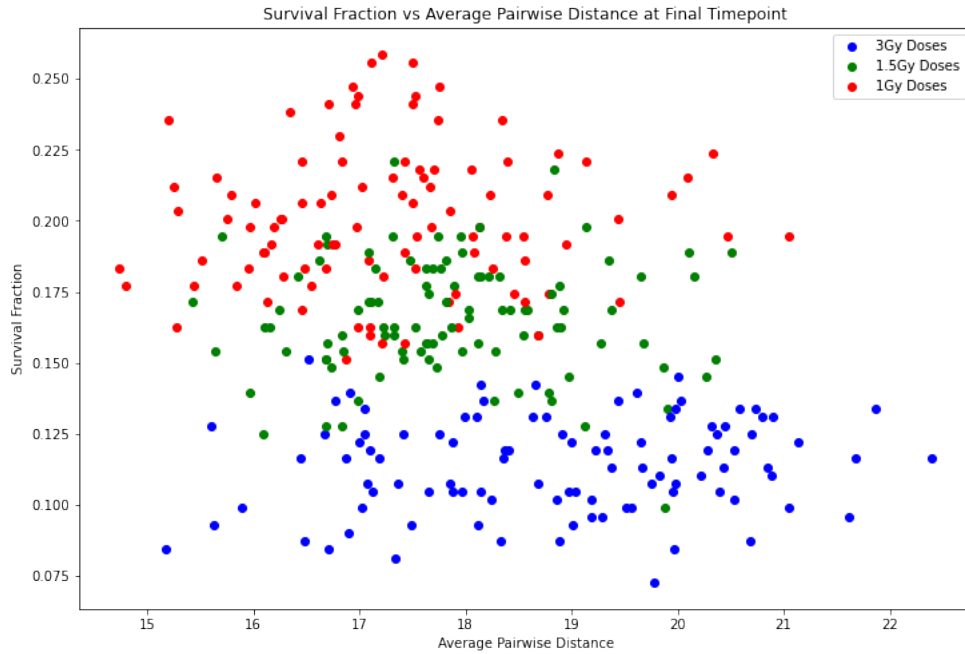


Figure 3.5: Analysis of hypo and hyperfractionated schedules in terms of both average pairwise distance and survival fraction.

As seen in Figure 3.5, there is indeed a trade-off between tumor dispersion and survival fraction. It seems that at hypofractionated schedules, there is more cell death but also results in more dispersion within the tumor. The increase in cell death is easily understood as it is directly related to the linear quadratic model, which has a dynamic that at dosage values, radiation kills increasing amounts of cells. Two possible explanations for why the hyperfractionated schedule has less dispersion than the hypofractionated schedule are effects of splitting up a larger dose over time and dynamics of the factor in dose combining.

When splitting up a larger dose over the course of a day, there are brief periods of time in which the average velocity of cells is relatively low, which falls in line with the result that there is less dispersion in the tumor. For example, on day 1, the velocity of the cells between 08:00 and 12:00 is only the velocity relating to one dose. When the second dose

is introduced at 12:00, there is then the velocity of two combined doses, and furthermore, until the third dose is given. During the course of this staggering, the average cell velocity is less than that of one full dose even before the dynamics of the diminishing returns in the model are taken into account. However, this staggering also has the effect of the final dose of a day having lingering effects throughout the following day, as the effects of a dose of radiation last for 24 hours. This certainly has some counter-effect in favor of increasing dispersion in the tumor.

Additionally, as described in the methods section, there is a diminishing returns factor, such that each subsequent dose within temporal proximity of each other has less of an effect on the average velocity of the tumor cells. In this analysis, the diminishing returns factor used is 0.5, which certainly has a major effect on the results. Since the hyperfractionated schedules will have diminishing effects on the velocity with each subsequent dose, it makes sense that these hyperfractionated schedules will have the end result that the tumor is less dispersed than the hypofractionated schedules.

3.4 Sensitivity Analyses

There were a number of important choices made while building the model, all of which could have effects on the results. This section explores the effects of the diminishing returns factor, and briefly discusses the effects of initial population size and simulation length.

In order to explore how much of an effect the diminishing returns factor has on the results, a factor sensitivity analysis was performed. In each of the schedules defined in the previous section (3Gy once a day, 1.5Gy twice a day, and 1Gy three times a day), the schedules were run under different values of the diminishing returns factor. The results are in Figure 3.6.

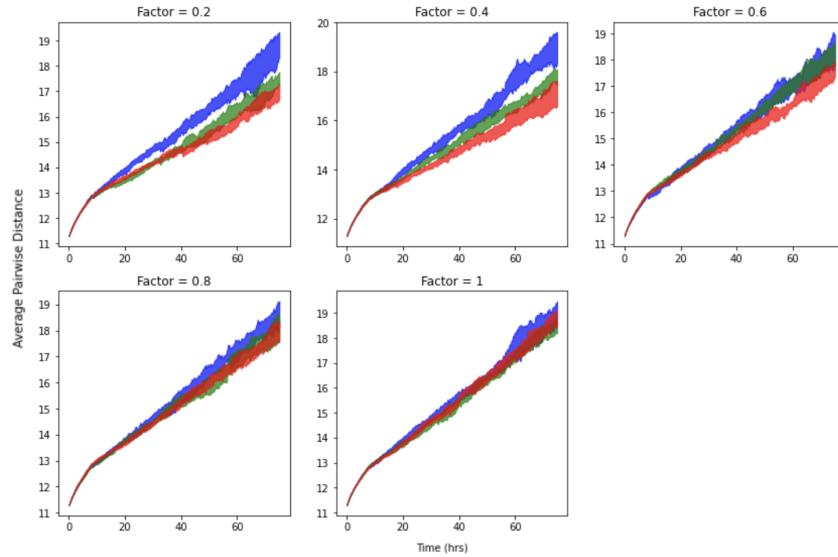


Figure 3.6: 3Gy once a day in blue, 1.5Gy twice a day in green, and 1Gy three times a day in red. Schedules run for 75 hours. Upper and lower bounds for schedules determined in the same manor as Figure 3.4

It can be seen from Figure 3.6, that the value of the diminishing returns factor has an important effect on the final dispersion of the tumor. At lower values of the diminishing returns factor, the difference between the three schedules is pretty large, but when the diminishing returns factor is 1, for example, the schedules are indistinguishable. This makes sense mathematically, as a diminishing returns system with a factor of one doesn't have any diminishing returns, but overall this analysis demonstrates the importance of the choice of the diminishing returns factor value in these analyses.

The effects of initial population size and simulation length were explored as well. Upon simulation, the initial population size did not have any significant effects on relative differences between schedules. This makes sense because radiation kills cells in fractions of the whole, so changing the initial population size will change the absolute amount of cells that are alive during the time course of radiation treatment, but it will have similar rela-

tive results to other schedules than at other initial population sizes. To explore simulation length, simulated tumors were looked at 2 weeks after the initial time point, with 5 day hypo/hyperfractionated schedules implemented in the first week. At the two week mark, since cells were allowed to freely grow, schedules were relatively indistinguishable from each other as a full-scale tumor was formed.

3.5 Optimization Algorithm

In order to find the optimal schedule, simulated annealing was used to explore the parameter space and find an optimal schedule. The basic premise of simulated annealing is to jump around the parameter space, in the beginning, to ensure that the algorithm doesn't get caught in a local optimum, and then slowly narrow in on the global optimum. This is done by use of what is called temperature. At each step of the algorithm, a new schedule is run 70 times and then scored. The way each schedule is scored is through the use of a z-score in relativity to the standard of care. The standard of care schedule was run for 80 replicates, and then the average and standard deviation of both the survival fraction and average pairwise distance were saved. When scoring a schedule, the standard error of the mean z-score, which follows the form

$$z = \frac{x - \mu}{(\sigma/\sqrt{n})} \quad (3.1)$$

is used in both the average pairwise distance and survival fraction dimension. In the formula, x is the average of the dimension of the new schedule, μ is the mean of the standard of care of the dimension, σ is the standard of deviation of the standard of care, and n is the number of replicates of the standard of care: 80. Then, the two z-scores of the two

dimensions are taken and averaged. The standard of care schedule would have a total score of 0. Importantly, if a score is negative, then that means that the scored schedule performs better than the standard of care in either one or both of average pairwise distance and survival fraction.

After the new schedule is scored, it is compared to the current schedule and the best schedule so far. If the new schedule is better than either the current schedule or the best schedule, then the new schedule will replace it. With high values of temperature, the new solution is more likely to randomly replace the current solution, but not the best solution. Then a new schedule is chosen based on the current schedule. This allows the algorithm to explore local optima and move the current schedule out of them, but still remember the local optima if it is able to replace the best schedule.

Each new schedule is chosen based on a certain distance from the current schedule. In order to choose a potential new solution that is close to the current schedule, Hamming distance is used. A Hamming distance of one away from a current schedule would mean that there is a difference in 1Gy somewhere in the schedule (1Gy subtracted from a particular dose time or 1Gy added to a different particular dose time). In general simulated annealing algorithms, this distance between new schedules and current schedules is constant throughout the entire algorithm, and the distance should be chosen such that the algorithm is able to traverse the entire parameter space just in case it starts out in a poor location. It is unclear what the best choice of Hamming distance between schedules is. In this algorithm, since each schedule must have 10Gy total, it is only possible to have schedules that are an even number of hamming distance away, since 1Gy must be subtracted from one dose time and then added to another dose time. In the algorithm, this adding and subtracting method was done 3 independent times, such that the total possible hamming distance between schedules

is 6Gy, but it is also possible to have hamming distances of 2 and 4Gy if the independent adding and subtracting were to choose the same dose times. Since there are 15 possible dose times, it is unlikely that the same dose times are chosen to add and subtract from, but still a possibility. The probability of such an occurrence is complicated by the fact that each new schedule must abide by the schedule constraints addressed in the exploration of practical radiation schedules section. For example, in calculating a new schedule, one can't add 1Gy to a dose time that already has 4Gy and one can't subtract 1Gy from a dose time that is already as 0Gy, as negative values of radiation don't exist. Therefore, the probability that adding and subtracting 1Gy 3 independent times ends up as less than a Hamming distance of 6Gy is greater than $3 * \frac{1}{15^2}$, but would have to be calculated on a per schedule basis, if calculated at all. Regardless, as seen in figure 10, the algorithm does converge to values less than 0, meaning that the algorithm has managed to find a parameter space in which it consistently finds schedules that have a z-score better than the standard of care.

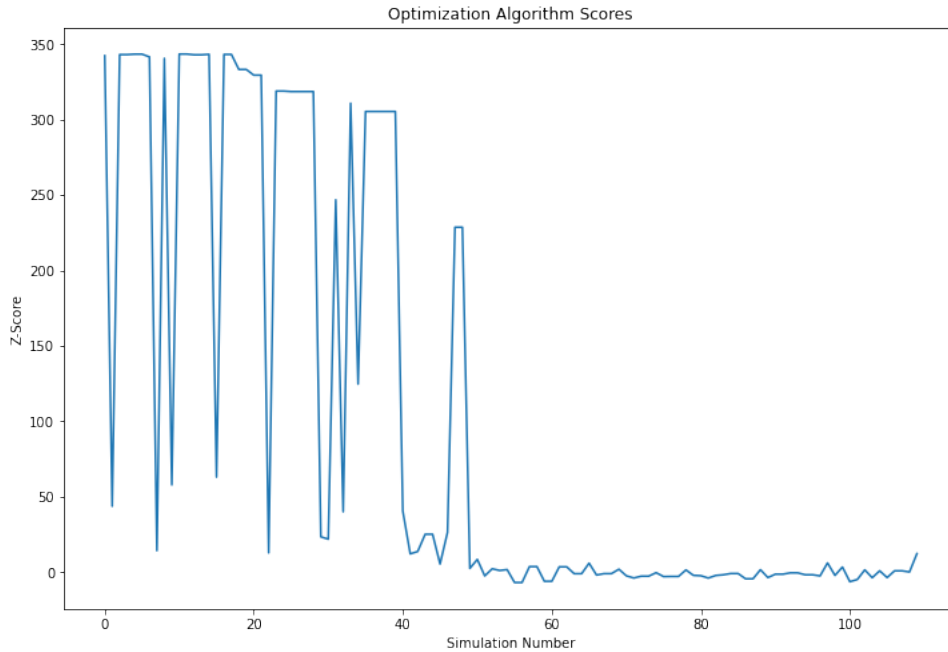


Figure 3.7: Progression of Simulated Annealing Algorithm

The optimal schedule found was having 2 doses of 4Gy in the first half of the schedule, at hour 16 and 56, followed by 2 1Gy doses later in the schedule, at hour 84 and 108. It is unclear what type of minimum this is, although it is a robust one, since the simulated annealing algorithm found it and remained in that space for the rest of the algorithm run time. A possible explanation is that the two 4Gy doses in the first half of the schedule killed off most of the tumor and then the 1Gy doses later in the schedule inhibit growth while not contributing too much to dispersion.

3.6 Negative Slope Analysis

An important feature of A549 cells in these analyses is that that the velocity of cells is positively correlated with increasing radiation dose. To further explore the realm of possi-

bilities that this project has begun to delve into, another NSCLC cell line was looked at. In the radiation dose-velocity data set [18], H460 was another cell line that was experimented with. It has a negative correlation with radiation dose, meaning that increased radiation actually led to a decrease in cell velocity. This dose-velocity relationship was plugged into the model, with the rest of the parameters remaining the same (and pertaining to A549). The same set of analysis as in Figure 3.4 were performed. The results are in Figure 3.8.

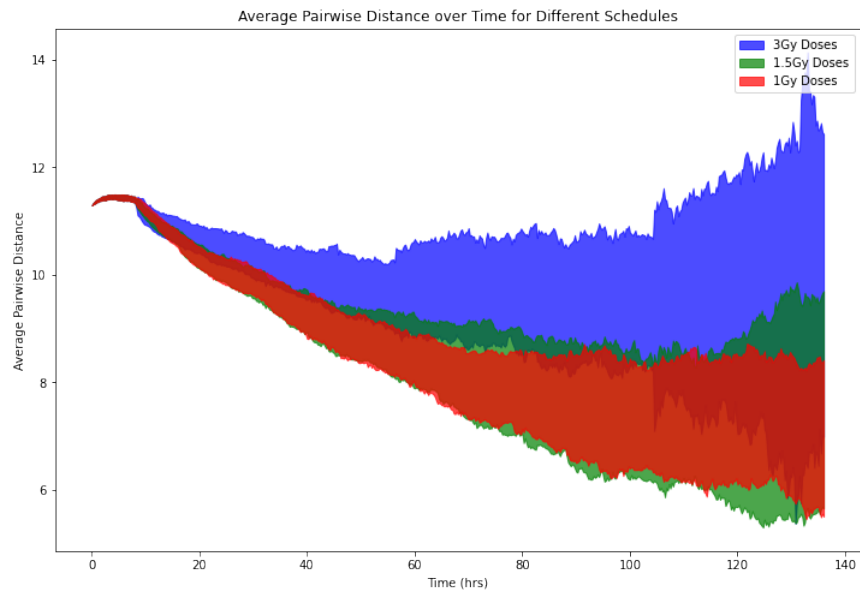


Figure 3.8: Average pairwise distance of tumor in response to hypo and hyperfractionated radiation schedules with a negative relationship between slope and increasing radiation dose.

Perhaps unexpectedly, there is still a similar trade-off dynamic in which the hypofractionated, 3Gy dose schedule leads to a more dispersed tumor, while the hyperfractionated, 1Gy dose schedule leads to less dispersion. Upon diving deeper into the simulation, it seems that this reasoning behind this has to do with the magnitude of velocity that H460 cells have in the data set. As compared to A549 cells, they are much slower, and while A549 cells were able to break apart from each other and move around, H460 cells weren't quite

able to break apart due to their natural lower speed. Therefore, radiation had the effect of splitting the cells apart from each other through the mechanism of random cell death, and since the 3Gy schedules kill more cells, which is known from Figure 3.5, this ended up in leaving the tumor in a more dispersed state.

Chapter 4

Conclusion

In this project, a quantification of the A549 cell line's motility response to radiation is used as a reflection of migration, and radiation schedules are explored and optimized to explore this new dynamic. In terms of novelty, to the best of the author's knowledge, this is the first time in which radiation schedules have been explored in such depth with a focus on cellular motility and migration.

First of all, it was demonstrated through the simulation of practical radiation schedules that the standard of care schedule performs well in terms of tumor death, but can be improved upon in terms of both tumor death and average pairwise distance of the cells. Upon diving deeper into radiation schedules themselves, it was established that hypofractionation can lead to more cell death, but it has the trade-off that it the tumor ends up in a more dispersed state. On the other hand, hyperfractionated schedules lead to less cell death but don't cause as much dispersion in the tumor. These results are complicated by important modeling choices, such as the diminishing returns system and the choice of the diminishing

returns factor value. Furthermore, a simulated annealing algorithm yielded a schedule that performed better than the standard of care both in terms of the z-scoring system used.

There are a variety of factors that must be taken into consideration when looking at the results of this project. First and foremost, the data from the Lahav lab that quantified the motility dose-response of A549 cells was done *in vitro* [18]. It is not clear what the results might be *in vivo*. Additionally, cellular motility and cellular migration are used in close proximity to each other throughout this project, but there is an important difference between the two. Namely, cellular motility simply refers to the motion of cells, while cell migration refers to cells moving to other parts of the body. In terms of what is dangerous, cancer cell migration is far more important. Although there is research to suggest that cellular motility plays an important role in migration [3], as discussed earlier, there is not a direct and established relationship between the dispersion metric used in this project and metastasis. However, in the case of A549 cells, it is known that there is both an increase in motility and migration in response to radiation [13] [12], so this project was designed to look at motility response with the thought that minimizing motility would be important for minimizing chances of migration and metastasis.

4.1 Further Directions

There are a variety of experiments and downstream analyses that can be performed to solidify the results of this project. One important thing is an exploration of how doses that are in close temporal proximity to each other affect the velocity. As discussed, the diminishing returns factor plays an important role in the results of the simulations, and experimentation to verify and explore this dynamic is important for understanding and contextualizing the results of this project.

An additional direction of this project would be to generalize this in terms of multiple lung cancer cell lines, as it is important to recognize that although A549 may be well studied, each cancer cell line has unique characteristics, and more cell lines need to be studied before making a general claim about lung cancer. Expanding this model to other cell lines and running optimization algorithms could lead to the identification of a schedule or concept of a schedule that could perform well regardless of the relationship that a specific cell line has with respect to cell velocity and radiation dose.

Bibliography

- [1] Zuzana Nova, Henrieta Skovierova, and Andrea Calkovska. Alveolar-capillary membrane-related pulmonary cells as a target in endotoxin-induced acute lung injury. *International Journal of Molecular Sciences*, 20(4), 2019.
- [2] Brittany Bowman. *FADD and its Phosphorylation Mediate Mitogenic Signaling in Mutant Kras Tumors*. PhD thesis, 05 2015.
- [3] Danny R Welch and Douglas R Hurst. Defining the hallmarks of metastasis. *Cancer research*, 79(12):3011–3027, 2019.
- [4] American Lung Association. Lung cancer fact sheet. <https://www.lung.org/lung-health-diseases/lung-disease-lookup/lung-cancer/resource-library/lung-cancer-fact-sheet>.
- [5] American Cancer Society. Key statistics for lung cancer. <https://www.cancer.org/cancer/lung-cancer/about/key-statistics.html>.
- [6] Johns Hopkins Medicine. Lung cancer types. <https://www.hopkinsmedicine.org/health/conditions-and-diseases/lung-cancer/lung-cancer-types>.
- [7] A549 cell line transfection, protocol, kits and reagents. <http://www.a549.com/>.

- [8] Cancer Treatment Centers of America. Lung cancer types. <https://www.cancercenter.com/cancer-types/lung-cancer/types>.
- [9] Geoff Delaney, Susannah Jacob, Carolyn Featherstone, and Michael Barton. The role of radiotherapy in cancer treatment: estimating optimal utilization from a review of evidence-based clinical guidelines. *Cancer: Interdisciplinary International Journal of the American Cancer Society*, 104(6):1129–1137, 2005.
- [10] Gillian C Barnett, Catherine ML West, Alison M Dunning, Rebecca M Elliott, Charlotte E Coles, Paul DP Pharoah, and Neil G Burnet. Normal tissue reactions to radiotherapy: towards tailoring treatment dose by genotype. *Nature Reviews Cancer*, 9(2):134–142, 2009.
- [11] Nora Sundahl, Frédéric Duprez, Piet Ost, Wilfried De Neve, and Marc Mareel. Effects of radiation on the metastatic process. *Molecular Medicine*, 24(1):1–20, 2018.
- [12] S. Ishihara, H. Haga, M. Yasuda, T. Mizutani, K. Kawabata, H. Shirato, and T. Nishioka. Integrin [beta]1-dependent invasive migration of irradiation-tolerant human lung adenocarcinoma cells in 3d collagen matrix. *Biochemical and Biophysical Research Communications*, 2010.
- [13] J. Jung, S. Hwang, J. Hwang, E. Oh, S. Park, and I Han. Ionising radiation induces changes associated with epithelial-mesenchymal transdifferentiation and increased cell motility of a549 lung epithelial cells. *European Journal of Cancer*, 2007.
- [14] Arthur W Lambert, Diwakar R Pattabiraman, and Robert A Weinberg. Emerging biological principles of metastasis. *Cell*, 168(4):670–691, 2017.

- [15] Sendurai A Mani, Wenjun Guo, Mai-Jing Liao, Elinor Ng Eaton, Ayyakkannu Ayyanan, Alicia Y Zhou, Mary Brooks, Ferenc Reinhard, Cheng Cheng Zhang, Michail Shipitsin, et al. The epithelial-mesenchymal transition generates cells with properties of stem cells. *Cell*, 133(4):704–715, 2008.
- [16] Christine L Chaffer, Janelle P Brennan, John L Slavin, Tony Blick, Erik W Thompson, and Elizabeth D Williams. Mesenchymal-to-epithelial transition facilitates bladder cancer metastasis: role of fibroblast growth factor receptor-2. *Cancer research*, 66(23):11271–11278, 2006.
- [17] Jeff H Tsai, Joana Liu Donaher, Danielle A Murphy, Sandra Chau, and Jing Yang. Spatiotemporal regulation of epithelial-mesenchymal transition is essential for squamous cell carcinoma metastasis. *Cancer cell*, 22(6):725–736, 2012.
- [18] Justin Dean, Ashwini Jambhekar, Adrian Granada, Jacob Stewart-Ornstein, Franziska Michor, and Jamie Dean. ... is associated with a treatment-induced increase in cell motility. *Unpublished*, 2020.
- [19] Amanda Randles, HG Wirsching, J Dean, S Emerson, SS Pattwell, EC Holland, and F Michor. Computational modeling of the glioblastoma microenvironment identifies optimum temozolomide-radiotherapy administration schedules. *Nature Biomedical Engineering*, 2021.
- [20] A A. Hill, LD Skarsgard. Cell-age heterogeneity and deviations from the lq model in the radiation survival responses of human tumour cells. *International journal of radiation biology*, 75(11):1409–1420, 1999.
- [21] KE Poels, AJ Schoenfeld, A Makhnin, Y Tobin, Y Wang, H Frisco-Cabanos, S Chakrabarti, M Shi, C Napoli, TO McDonald, W Tan, A Hata, SL Weinrich, HA Yu,

- and Michor F. Identification of optimal dosing schedules of dacomitinib and osimertinib for a phase i/ii trial in advanced egfr-mutant non-small cell lung cancer. *Nature Communications*, 2021.
- [22] Lucyna Kepka and Joanna Socha. Dose and fractionation schedules in radiotherapy for non-small cell lung cancer. *Translational Lung Cancer Research*, 10(4), 2020.
- [23] Michelle Iocolano, Aaron T Wild, Margaret Hannum, Zhigang Zhang, Charles B Simone, Daphna Gelblum, Abraham J Wu, Andreas Rimner, and Annemarie F Shepherd. Hypofractionated vs. conventional radiation therapy for stage iii non-small cell lung cancer treated without chemotherapy. *Acta Oncologica*, 59(2):164–170, 2020.